Signal processing of phase image timeseries to remove respiratory and cardiac noise in functional susceptibility mapping

R. Allen Waggoner
Support Unit for Functional Magnetic Resonance Imaging
RIKEN Center for Brain Science
Wakoshi, Japan
raw@riken.jp

Oliver C. Kiersnowski
Neuroradiology Unit
Ospedale Policlinico San Martino
Genoa, Italy
https://orcid.org/0000-0001-6016-0514

Kenichi Ueno
Support Unit for Functional Magnetic Resonance Imaging
RIKEN Center for Brain Science
Wakoshi, Japan
uken@riken.jp

Luca Roccatagliata
Department of Health Sciences
University of Genoa
Genoa, Italy
https://orcid.org/0000-0001-8029-3947

Chisato Suzuki
Support Unit for Functional Magnetic Resonance Imaging
RIKEN Center for Brain Science
Wakoshi, Japan
chisato.suzuki@riken.jp

Mauro Costagli
Department of Neuroscience, Rehabilitation, Ophthalmology, Genetics, Maternal and Child Health
University of Genoa
Genoa, Italy
https://orcid.org/0000-0001-9073-1082

***Abstract*—This study aims to assess the impact of physiological noise, introduced by respiratory and cardiac cycles, in phase images acquired with functional magnetic resonance imaging (fMRI), which are the main input for functional quantitative susceptibility mapping (fQSM). We demonstrated that retrospective physiological noise correction reduces the temporal variance of phase image timeseries. We showed the impact of respiratory and cardiac noise correction at different stages of the fQSM pipeline, focusing on the following regions of interest: the visual cortex, the auditory cortex and the brainstem. Physiological noise correction, quantified in terms of the ratio between the temporal variance of the corrected and uncorrected timeseries, exhibited a large dependence on the acquisition echo time in phase images. The dominant noise component originated from respiration. At later stages of the fQSM processing pipeline, the impact of noise ascribable to the cardiac cycle became dominant, especially at short echo times. The brainstem exhibited the largest effects of cardiac noise correction. Our results suggest that, in the challenging context of fQSM, physiological noise correction may be a necessary preprocessing step, more than in conventional fMRI, especially when the target regions include brain areas largely affected by respiratory and cardiac-related noise, such as the brainstem.**

Keywords—magnetic resonance imaging, brain activity, functional MRI, magnetic susceptibility, quantitative susceptibility mapping, functional QSM, physiological noise, respiration noise, cardiac noise

I. Introduction

Quantitative susceptibility mapping (QSM) is a recently established technique enabling a quantitative assessment of biological tissues' magnetic susceptibility using Magnetic Resonance Imaging (MRI) phase images as input data [1]. The rationale of QSM and the necessary steps to achieve it are illustrated in detail in the literature [2], and are summarized as follows.

This study was supported by the Japanese Society for the Promotion of Science (JSPS), Fellowship ID S23130.

In the presence of an external, homogeneous magnetic field B_0, protons precess with frequency $\omega_0 = \gamma \cdot B_0$, where $\gamma = 42.577$ MHz/T is the gyromagnetic ratio of the proton. However, small, local magnetic field perturbations ΔB are caused by the spatial distribution of tissues with different magnetic susceptibilities χ, convolved with the known unit magnetic dipole kernel d, that is, the mathematical expression describing the magnetic field generated by a point-like susceptibility source in its surrounding space.

Local field inhomogeneities are described by the following equation:

$$\Delta B(r) = B_0 \cdot [\chi(r) \otimes d(r)], \quad (1)$$

where r represents the vector of spatial coordinates and $\otimes$ indicates the convolution operation. Such field perturbations ΔB do not precisely co-localize with the magnetic susceptibility sources; instead, perturbations extend beyond their sources due to the convolution operation with the dipole kernel. Information on the spatial distribution of field inhomogeneities is contained in the phase of the complex-valued gradient-echo MRI signal obtained at a specific Time of Echo (TE):

$$\varphi(r, TE) = \gamma \cdot \Delta B(r) \cdot TE + \varphi_0(r), \quad (2)$$

where TE is the Time of Echo (that is, the time when the MR signal is read after excitation) and φ_0 is the phase at TE = 0. A map of $\chi(r)$ is finally obtained via deconvolution of the dipole kernel.

A. Functional MRI

The study of magnetic susceptibility is relevant in a wide range of applications, including clinical studies targeting biological tissues with different χ (for example, tissues with different concentrations of iron, lipids, calcium) [3], and functional MRI (fMRI), which is the focus of this research. In fact, fMRI relies on the varying relative concentrations of oxygenated and deoxygenated hemoglobin (which have

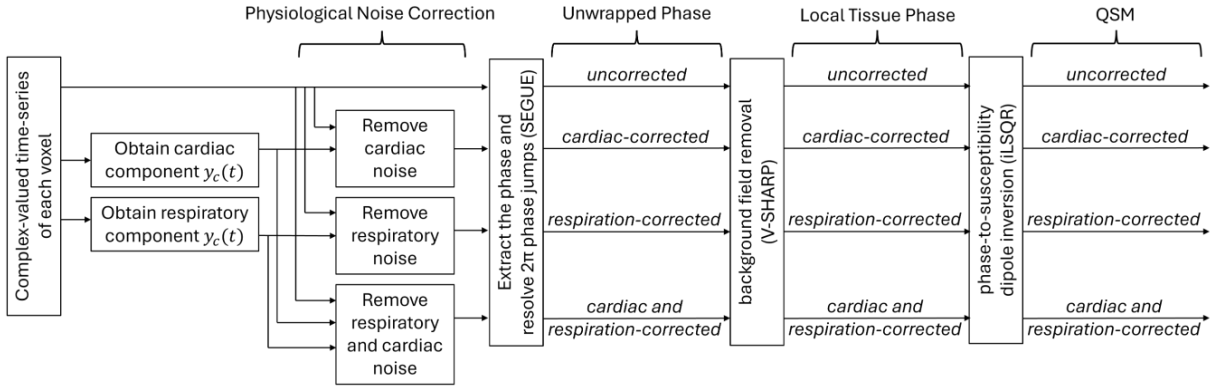

Fig. 1. Scheme of the processing pipeline, including physiological noise correction of the complex-valued input data and further processing of phase images

different magnetic susceptibilities) in the blood, in response to neural activity, that is, the so-called Blood-Oxygenation Level Depended (BOLD) effect [4]. Conventional BOLD-fMRI aims to identify neural activity on the basis of local changes in the magnitude of the complex-valued MRI signal, which follows the temporal fluctuations of local field inhomogeneity related to the varying concentrations of oxy- and deoxy-hemoglobin. Following the considerations above, the information provided by conventional BOLD-fMRI is not well localized (as field perturbations involve the neighborhood of the magnetic susceptibility source) and not quantitative.

B. Functional Quantitative Susceptibility Mapping

Functional QSM (fQSM) is a recent extension of traditional QSM to functional brain mapping [5], [6], [7], [8], [9], [10], [11], [12], [13]. Data for fQSM is typically obtained using a 2D Echo-Planar Imaging (EPI) MRI sequence, which is the same acquisition sequence used for conventional fMRI-BOLD. However, instead of identifying activations based on changes in the signal magnitude, fQSM leverages on the information embedded in the MR signal phase and offers additional information to that of BOLD contrast. The main advantages of fQSM over fMRI include providing a quantitative measure of magnetic susceptibility changes over time, and its images are virtually void of the spurious, nonlocal signal alterations that are commonly present in conventional fMRI. Taken together, these two properties enable fQSM to provide a quantitative assessment of a precisely localized response.

C. Physiological noise in functional MRI

Information in BOLD-fMRI is carried by small fluctuations of the MR signal magnitude, typically consisting of around 2% signal change in noisy timeseries. fQSM is even more challenging, considering that in fQSM the spatially smooth signal components, inherent to fMRI and beneficial for activity detection, are absent. It follows that improving the fQSM quality, for example by removing noise components, is particularly important.

Functional MRI data are affected by unavoidable physiological noise arising from respiration and cardiac cycles, which can reduce the visibility of true neuronal activation and sometimes appear as false activations themselves. In this context, one possible denoising approach is to resort to physiological noise modelling, for example with the well-established RETROspective Image CORrection (RETROICOR) approach that utilizes external recordings of the cardiac and respiratory signals [14]. In short, RETROICOR assumes that the physiological processes of the cardiac and respiratory cycles are quasi-periodic and phase values φ_c and φ_r, ranging between 0 and 2π, can be assigned to each 2D image depending on the temporal position of the acquired image, relative to cardiac and respiratory cycles, respectively. For example, the cardiac phase of a frame acquired at time t_a is:

$$\varphi_c(t_a) = 2\pi \cdot (t_a - t_p)/(t_s - t_p) \qquad (3)$$

where t_p is the time of the R-wave peak in the cardiac cycle preceding t_a, while t_s is the time or the subsequent R-wave peak. φ_r is assigned similarly, relative to the respiratory cycle. It follows that the physiological noise components relative to the cardiac cycle, $y_c(t)$, and the respiratory cycle, $y_r(t)$, can be expressed as a low-order Fourier series expanded in terms of these phases. For example, for the cardiac component:

$$y_c(t) = \sum_{m=1}^{M}[a_m^c \cos(m\varphi_c) + b_m^c \sin(m\varphi_c)] \qquad (4)$$

where M is typically set to 2 [14]. This approach assumes that no other temporal modulations share the same periodicity as the cardiac or respiratory cycles. For resting-state or block-design fMRI, this assumption generally holds. However, in event-related fMRI, careful task design is essential to ensure that the task temporal structure differs sufficiently from the cardiac and respiratory rhythms. The impact of physiological noise is known to affect EPI phase to a greater extent than the magnitude signal [15], [16]; however, the effect of physiological noise correction on EPI-phase and fQSM has not been thoroughly investigated.

In this study, we investigate the effects of respiratory and cardiac noise correction on the EPI phase at different stages through the QSM pipeline, and in different brain regions that may be differently impacted by physiological noise.

II. Materials and Methods

Multi-echo 2D-EPI magnitude and phase data were acquired on a MAGNETOM Prisma 3T MRI system. Four healthy volunteers (average age, 47.2 years; all males) were presented with flickering checkerboard visual stimuli, with a stimulus duration of 0.5 s and inter-stimulus intervals of either 16 s or 24 s over three consecutive runs consisting of 205, 200 and 205 frames, respectively. For each volume, Times of Echo

(TE) were 14.4, 35.3, 56.1, 77.0 ms; Time of Repetition (TR) was 1.6 s; voxel size was 2 mm isotropic with matrix size = 110×110×60; multiband factor = 4; parallel imaging acceleration with Generalized Autocalibrating Partially Parallel Acquisitions (GRAPPA) [17] was used, with GRAPPA factor = 3; partial Fourier = 7/8.

Pulse oximetry and respiratory data were acquired simultaneously with the EPI acquisitions using a BioPac MP150 system. Physiological noise correction was applied using an in-house RETROICOR program on the real and imaginary components of the complex-valued images on a voxel-wise basis, as schematically represented in Fig. 1. Then, the phase images were extracted from the uncorrected and noise-corrected complex-valued images, the latter consisting of three sets of data where *i)* only cardiac correction, *ii)* only respiration correction, and *iii)* respiratory followed by cardiac noise correction were applied. For each frame and echo, 2π ambiguities in phase images were resolved using SEGUE (Speedy rEgion-Growing algorithm for Unwrapping Estimated phase) [18].

Further processing, common to all four sets of unwrapped phase images, included the removal of low spatial frequency field inhomogeneities related to large magnetic susceptibility differences of no interest (e.g., between the magnetic susceptibility of brain tissues and air) by applying 2D+3D variable-kernel sophisticated harmonic artifact reduction for phase data (V-SHARP) [19], which resulted in local tissue phase maps. The phase-to-susceptibility operation was achieved with the iterative least squares (iLSQR) method [20], which resulted in the final fQSM data (Fig. 1).

The metric used to assess the impact of physiological noise correction (PNC) is the relative variance σ_r^2, which is calculated voxel-wise as the ratio between the temporal variance after PNC and the temporal variance before correction:

$$\sigma_r^2 = \sigma_{afterPNC}^2 / \sigma_{beforePNC}^2 \quad (5)$$

The expected values of σ_r^2 are in the range [0, 1], with lower values indicating more effective PNC. This metric was calculated separately for the four echoes, at different steps of the QSM pipeline: on the unwrapped phase, on the local tissue phase and on the final fQSM data. The relative variance was computed within the whole brain mask obtained with the Brain Extraction Tool (BET) [21], as well as in the following regions of interest (ROI): the visual cortex and auditory cortex, obtained from the Juelich MNI template [22], and in the brainstem, obtained from the Talairach MNI template [23].

III. Results

The amount of temporal variance removed by physiological noise correction was quantified at different steps of the fQSM pipeline, as described in the subsections below.

A. Impact of PNC in the unwrapped phase

In the unwrapped phase images, the amount of removed variance exhibited echo dependence, with smaller σ_r^2 (that is, larger impact of physiological noise) at longer TE than at the shortest TE. In the visual cortex, the average σ_r^2 varied between 0.83 and 0.72 with TE, while in the auditory cortex it varied between 0.87 and 0.74. In the whole brain mask, however, average σ_r^2 varied less with TE, ranging between 0.83 and 0.80. The most part of removed variance was ascribable to respiration noise. The impact of cardiac noise was minimal and exhibited a less clear TE dependence globally, throughout the whole brain, but clear, localized effects were visible near vessels and the brainstem. Fig. 2 highlights this behavior across the whole brain for one representative subject and presents quantitative values of relative variance calculated in the visual cortex, auditory cortex, and brainstem. In the brainstem, the set of images acquired at the longest TE exhibited $\sigma_r^2 > 1$ for the data

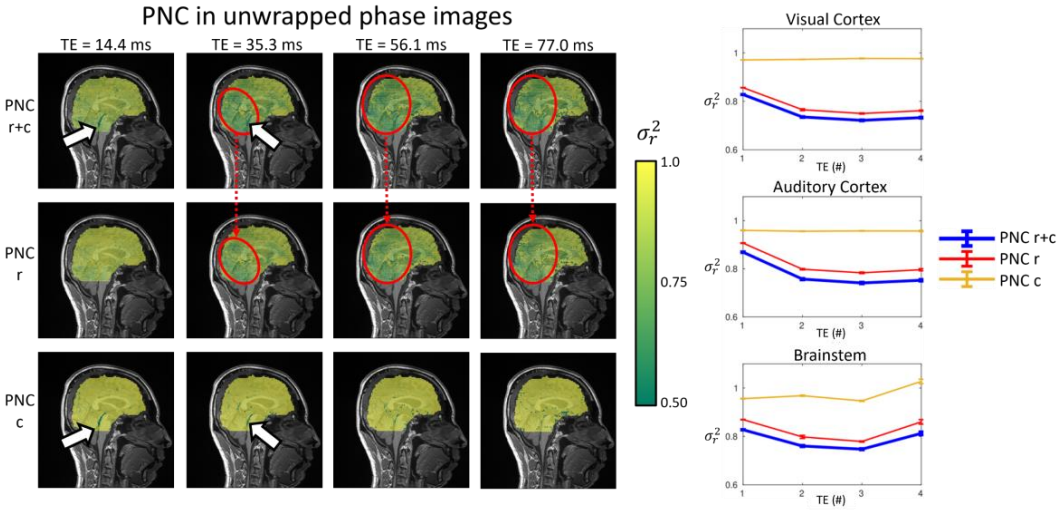

Fig. 2. The impact of physiological noise correction (PNC), mapped in terms of relative variance, σ_r^2, i.e. the voxelwise temporal variance reduction relative to the uncorrected data, in the unwrapped phase images of one representative subject. The colored maps in first row, overlaid onto an anatomical scan, represent σ_r^2 when both respiratory and cardiac noise correction and applied, for the four echo times. The second and third row represent σ_r^2 when only either respiration or cardiac noise correction are applied, respectively. Images obtained with longer TE exhibit the largest global impact of PNC. Large scale effects involving the whole brain are ascribed to respiration (examples indicated by red circles), while localized effects in the region of the brainstem are most prominent at short TE and are related to cardiac noise (white arrows). Plots on the right side of the figure indicate σ_r^2 in the visual cortex (top), auditory cortex (middle) and brainstem (bottom) when both respiratory and cardiac noise correction are applied (blue), as well as when only either respiration (red) or cardiac (yellow) noise corrections are applied

corrected only for cardiac noise. No apparent difference in the impact of PNC was observed between the visual cortex and the surrounding cortex, suggesting that PNC does not misidentify the visual response as cardiac or respiratory noise.

B. Impact of PNC in the local tissue phase

In the local tissue phase images after the V-SHARP step, respiratory noise and cardiac noise had a similar impact across the whole brain. The amount of removed variance is mapped in Fig. 3 for the subject shown also in Fig. 2. The global effects of respiration noise which were dominant in Fig. 2, here are absent, given that at this processing stage the low spatial frequency components are removed. Locally, the most pronounced effects of physiological noise are in the vicinity of the brainstem, where σ_r^2 exhibits values as low as 0.16 especially at shorter TE, related to cardiac noise. Values of σ_r^2 in the local tissue phase calculated in the visual cortex, auditory cortex, and brainstem, for different values of TE, are also shown. It is worth noting that in the brainstem the set of images acquired at the longest TE exhibited $\sigma_r^2 > 1$ for the data corrected for only either respiratory or cardiac noise.

C. Impact of PNC in the functional QSM

In QSM images, σ_r^2 in the whole brain mask was, on average, 0.96 and did not exhibit TE dependence. The correction of either respiratory or cardiac noise contributed equally in terms of average relative variance across the whole brain, as displayed in Fig. 4 for the subject shown also in Fig. 2 and 3. Different patterns of localized σ_r^2 reduction were observed near the brainstem, orbitofrontal cortex and near blood vessels. The most remarkable reduction in temporal variance was observed near the brainstem for shorter TE and was ascribable to cardiac noise.

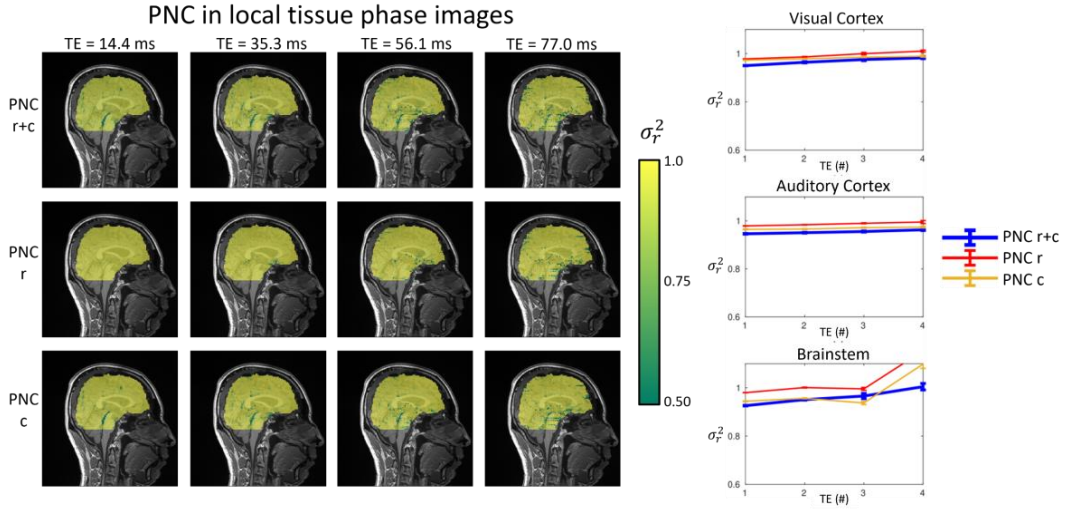

Fig. 3. The impact of physiological noise correction (PNC) represented in terms of relative variance maps in local tissue phase images (left) for the same subject shown also in Fig.2. Plots on the right side of the figure indicate σ_r^2 in three regions of interest when both respiratory and cardiac noise correction are applied (blue), as well as when only either respiration (red) or cardiac (yellow) noise corrections are applied

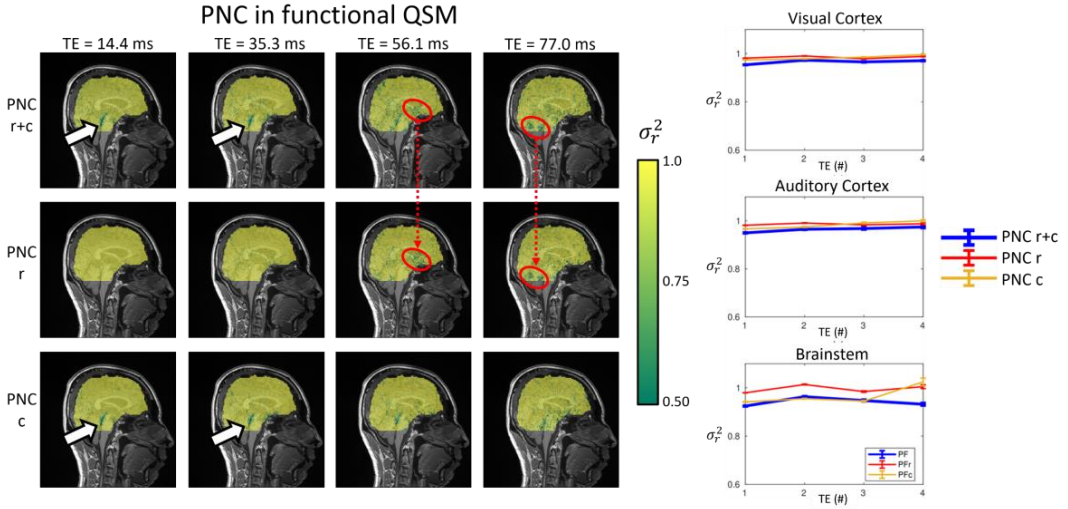

Fig. 4. The impact of physiological noise correction (PNC), mapped in terms of relative variance in functional QSM data (left) for the same subject shown also in Fig.2 and Fig.3. Localized effects related to cardiac noise are most prominent at short TE (white arrows), while effects related to respiration noise are most prominent at longer TE (red circles). Plots on the right side of the figure indicate σ_r^2 in three regions of interest when both respiratory and cardiac noise correction are applied (blue), as well as when only either respiration (red) or cardiac (yellow) noise corrections are applied

IV. Discussion and Conclusion

Functional quantitative susceptibility mapping relies on phase image timeseries. This study shows that physiological noise due to the respiratory and cardiac cycles markedly affects phase image timeseries, more than conventional BOLD timeseries relying only on the fMRI signal magnitude. Here we demonstrated that retrospective physiological noise correction via RETROICOR is capable of reducing the temporal variance of phase image timeseries, and we showed the impact of respiratory and cardiac noise correction at different stages of the fQSM pipeline. Physiological noise correction in phase images after the unwrapping step exhibits a large TE dependence, with the impact of correction increasing with TE, as quantitatively measured in terms of relative temporal variance of the timeseries. The dominant noise component originates from respiration: gross magnetic susceptibility changes, as the lungs inflate and deflate, produce large-scale magnetic field fluctuations in the brain. At later stages of the fQSM processing pipeline, the low spatial frequencies are filtered out and the impact of pulsatile motion and flow-related noise ascribable to the cardiac cycle becomes dominant, especially at short echo times. Among the regions of interest that were investigated in this study, the brainstem exhibited the largest effects of cardiac noise correction. We observed values of $\sigma_r^2 > 1$, mostly in the local tissue phase images acquired with the longest echo time in the brainstem region, suggesting the amplification of noise components correlated with respiration and cardiac cycles. It is likely that such noise components arise from tissue displacement with respect to voxel location, that is, they are a consequence of actual pulsatile motion which is not corrected for in this pipeline.

To the best of our knowledge, this is the first study targeting the effects of physiological noise correction throughout the fQSM pipeline. Our observations suggest that physiological noise correction may be an important step in the fQSM processing pipeline to improve the quality of such a challenging type of data. Future work will investigate the effects of physiological noise correction on fQSM activation maps representing the brain response to a cognitive task.

References

[1] A. Deistung, F. Schweser, and J. R. Reichenbach, 'Overview of quantitative susceptibility mapping', *NMR in Biomedicine*, vol. 30, no. 4, Apr. 2017, doi: 10.1002/nbm.3569.

[2] B. Bilgic *et al.*, 'Recommended implementation of quantitative susceptibility mapping for clinical research in the brain: A consensus of the ISMRM electro-magnetic tissue properties study group', *Magnetic Resonance in Medicine*, vol. 91, no. 5, pp. 1834–1862, 2024, doi: 10.1002/mrm.30006.

[3] Y. Wang *et al.*, 'Clinical quantitative susceptibility mapping (QSM): Biometal imaging and its emerging roles in patient care', *Journal of Magnetic Resonance Imaging*, vol. 46, pp. 951–971, 2017. doi: 10.1002/jmri.25693.

[4] J. M. Soares *et al.*, 'A Hitchhiker's Guide to Functional Magnetic Resonance Imaging', *Front. Neurosci.*, vol. 10, Nov. 2016, doi: 10.3389/fnins.2016.00515.

[5] Z. Chen, J. Liu, and V. D. Calhoun, 'Susceptibility-based functional brain mapping by 3D deconvolution of an MR-phase activation map', *Journal of Neuroscience Methods*, vol. 216, no. 1, pp. 33–42, May 2013, doi: 10.1016/j.jneumeth.2013.03.003.

[6] D. Z. Balla *et al.*, 'Functional quantitative susceptibility mapping (fQSM)', *NeuroImage*, vol. 100, pp. 112–124, Oct. 2014, doi: 10.1016/j.neuroimage.2014.06.011.

[7] M. Bianciardi, P. van Gelderen, and J. H. Duyn, 'Investigation of BOLD fMRI resonance frequency shifts and quantitative susceptibility changes at 7 T', *Human Brain Mapping*, vol. 35, no. 5, pp. 2191–2205, 2014, doi: 10.1002/hbm.22320.

[8] Z. Chen and V. Calhoun, 'Intrinsic functional brain mapping in reconstructed 4D magnetic susceptibility (χ) data space', *Journal of Neuroscience Methods*, vol. 241, pp. 85–93, Feb. 2015, doi: 10.1016/j.jneumeth.2014.12.014.

[9] P. S. Özbay *et al.*, 'Probing neuronal activation by functional quantitative susceptibility mapping under a visual paradigm: A group level comparison with BOLD fMRI and PET', *NeuroImage*, vol. 137, pp. 52–60, 2016, doi: 10.1016/j.neuroimage.2016.05.013.

[10] H. Sun, P. Seres, and A. h. Wilman, 'Structural and functional quantitative susceptibility mapping from standard fMRI studies', *NMR in Biomedicine*, vol. 30, no. 4, p. e3619, 2017, doi: 10.1002/nbm.3619.

[11] M. Costagli *et al.*, 'Quantitative Susceptibility Mapping of Brain Function During Auditory Stimulation', *IEEE Transactions on Radiation and Plasma Medical Sciences*, vol. 3, no. 4, pp. 516–522, 2019, doi: 10.1109/trpms.2019.2894262.

[12] C.-M. Shih, H.-C. Lo, M.-C. Hsieh, and J.-H. Chen, 'Functional quantitative susceptibility mapping (fQSM) of rat brain during flashing light stimulation', *NeuroImage*, vol. 233, p. 117924, Jun. 2021, doi: 10.1016/j.neuroimage.2021.117924.

[13] M. Lancione *et al.*, 'Complementing canonical fMRI with functional Quantitative Susceptibility Mapping (fQSM) in modern neuroimaging research', *NeuroImage*, vol. 244, p. 118574, Dec. 2021, doi: 10.1016/J.NEUROIMAGE.2021.118574.

[14] G. H. Glover, T.-Q. Li, and D. Ress, 'Image-based method for retrospective correction of physiological motion effects in fMRI: RETROICOR', *Magnetic Resonance in Medicine*, vol. 44, no. 1, pp. 162–167, 2000, doi: 10.1002/1522-2594(200007)44:1<162::AID-MRM23>3.0.CO;2-E.

[15] G. E. Hagberg, M. Bianciardi, V. Brainovich, A. M. Cassarà, and B. Maraviglia, 'The effect of physiological noise in phase functional magnetic resonance imaging: from blood oxygen level-dependent effects to direct detection of neuronal currents', *Magnetic Resonance Imaging*, vol. 26, no. 7, pp. 1026–1040, Sep. 2008, doi: 10.1016/j.mri.2008.01.010.

[16] N. Petridou, A. Schäfer, P. Gowland, and R. Bowtell, 'Phase vs. magnitude information in functional magnetic resonance imaging time series: toward understanding the noise', *Magnetic Resonance Imaging*, vol. 27, no. 8, pp. 1046–1057, Oct. 2009, doi: 10.1016/j.mri.2009.02.006.

[17] M. A. Griswold *et al.*, 'Generalized autocalibrating partially parallel acquisitions (GRAPPA)', *Magnetic Resonance in Medicine*, vol. 47, no. 6, pp. 1202–1210, Jun. 2002, doi: 10.1002/mrm.10171.

[18] A. Karsa and K. Shmueli, 'SEGUE: A Speedy rEgion-Growing Algorithm for Unwrapping Estimated Phase', *IEEE Transactions on Medical Imaging*, vol. 38, no. 6, pp. 1347–1357, Jun. 2019, doi: 10.1109/TMI.2018.2884093.

[19] H. Wei, Y. Zhang, E. Gibbs, N.-K. Chen, N. Wang, and C. Liu, 'Joint 2D and 3D phase processing for quantitative susceptibility mapping: application to 2D echo-planar imaging', *NMR in Biomedicine*, vol. 30, no. 4, p. e3501, Apr. 2017, doi: 10.1002/nbm.3501.

[20] W. Li *et al.*, 'A method for estimating and removing streaking artifacts in quantitative susceptibility mapping', *NeuroImage*, vol. 108, pp. 111–122, 2015, doi: 10.1016/j.neuroimage.2014.12.043.

[21] S. M. Smith, 'Fast robust automated brain extraction', *Human Brain Mapping*, vol. 17, no. 3, pp. 143–155, Nov. 2002, doi: 10.1002/hbm.10062.

[22] K. Amunts, H. Mohlberg, S. Bludau, and K. Zilles, 'Julich-Brain: A 3D probabilistic atlas of the human brain's cytoarchitecture', *Science*, vol. 369, no. 6506, pp. 988–992, Aug. 2020, doi: 10.1126/science.abb4588.

[23] V. Fonov, A. Evans, R. McKinstry, C. Almli, and D. Collins, 'Unbiased nonlinear average age-appropriate brain templates from birth to adulthood', *NeuroImage*, vol. 47, p. S102, Jul. 2009, doi: 10.1016/S1053-8119(09)70884-5.